ADVANCED MATERIALS

Supporting Information

for *Adv. Mater.,* DOI: 10.1002/adma.202103471

Engineering Extracellular Vesicles Enriched with Palmitoylated ACE2 as COVID-19 Therapy

Feng Xie, Peng Su, Ting Pan, Xiaoxue Zhou, Heyu Li, Huizhe Huang, Aijun Wang, Fangwei Wang, Jun Huang, Haiyan Yan, Linghui Zeng, Long Zhang, and Fangfang Zhou**

Supplementary Figure legends

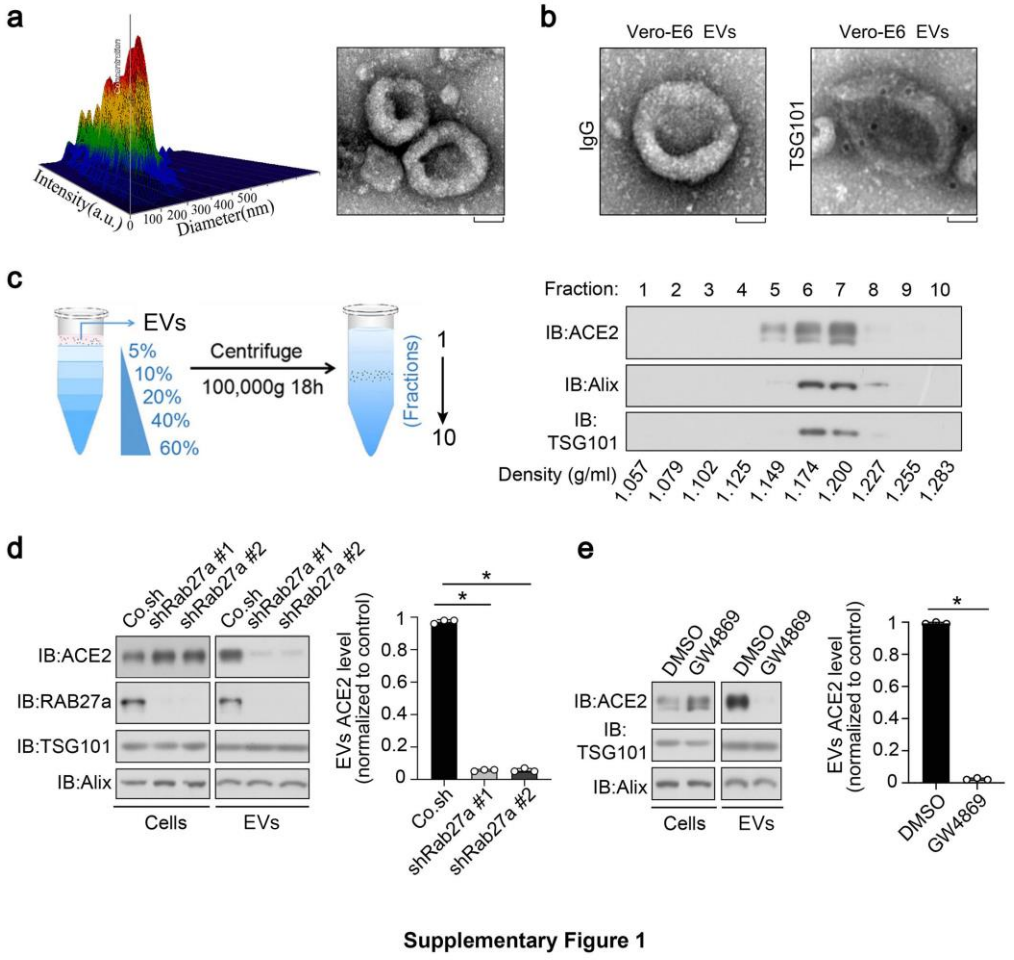

Supplementary Figure 1

Supplementary Figure 1. ACE2-expressing cells release EVs carrying ACE2. **a**, Nanoparticle tracking of purified EVs (left), and a representative TEM image of purified EVs (right) from Vero-E6 cells. Scale bar, 100 nm. **b**, TEM images of Vero-E6 cell lines-derived EVs immunogold-labeled with control IgG and anti-ACE2 antibodies. Scale bar, 50 nm. **c**, Schematic diagram of sucrose density gradient centrifugation for EVs purification (left) and immunoblot (IB) analysis of ACE2 expression in EVs (right). **d**, IB analysis (left) and quantification (right) of whole cell lysates and purified EVs derived from Vero-E6 cells stably depleted Rab27a by two independent shRNAs (sh Rab27a #1 and #2). **e**, IB analysis (left) and quantification

(right) of whole cells lysate and EVs derived from Vero-E6 cells treated with control DMSO or GW4869 (10 μM) for 48 h.

*$p < 0.05$ (two-tailed Student's t test (**d** (right), **e** (right)). Data are analyzed of three independent experiments and shown as mean ± SD (**d** (right)**, e** (right)).

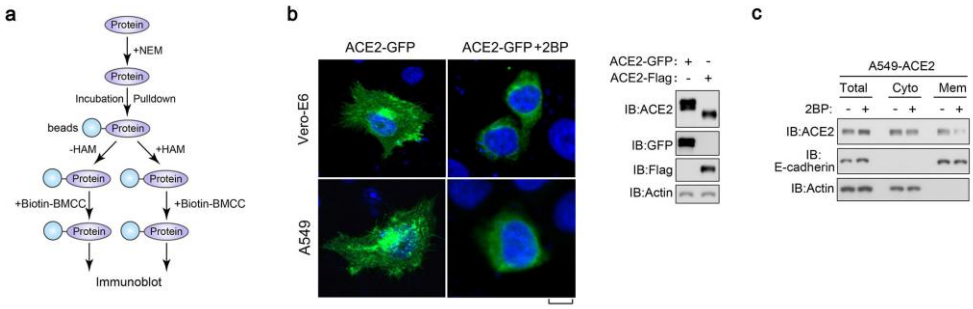

Supplementary Figure 2

Supplementary Figure 2. ACE2 S-palmitoylation is required for its membrane localization.

a, Schematic diagram of a S-palmitoylation detection method based on acyl-biotin exchange (ABE) assays. **b**, Left panel: immunofluorescence and DAPI staining of Vero-E6 and A549 cells transfected with ACE2-GFP and treated with control DMSO or 2BP (50 μM) for 24 h. Scale bar, 20 μm. Right panel: IB analysis of total cell lysate from HEK293T cells transfected with ACE2-GFP or ACE2-Flag. **c**, IB analysis of the total cell lysate (Total), cytosolic (Cyto) and membrane (Mem) fractions derived from A549 cells treated with control DMSO or 2BP (50 μM) for 24 h.

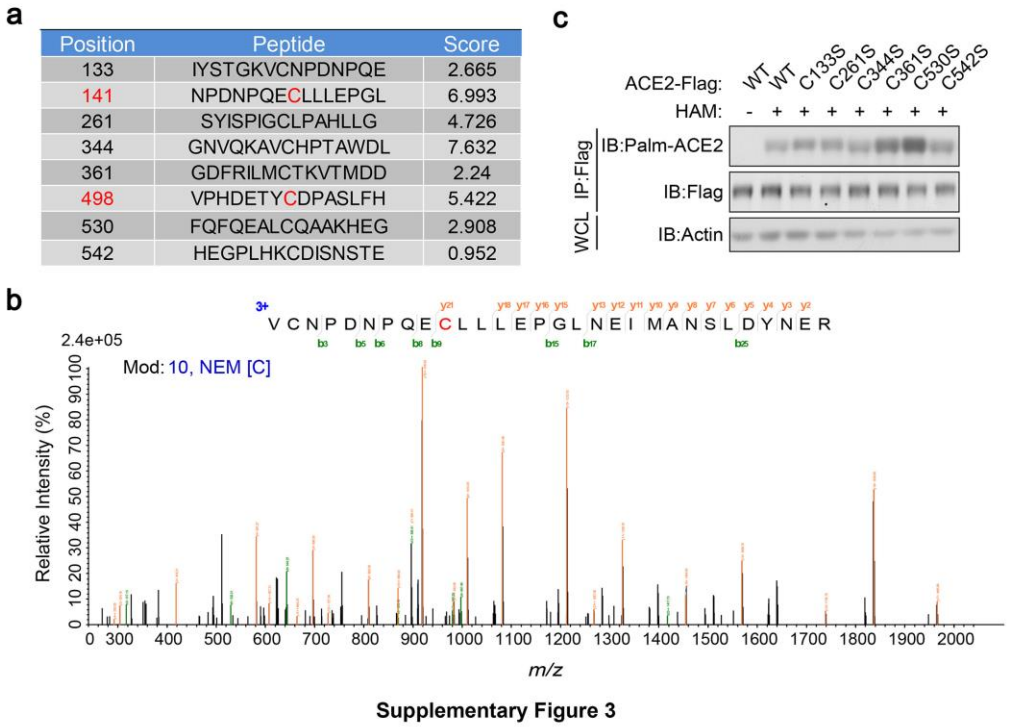

Supplementary Figure 3

Supplementary Figure 3. Identification of ACE2 palmitoylation sites.

a, The palmitoylation positions and scores of human ACE2 predicted by CSS-Palm. **b**,MS/MS spectrum of the $[M+2H]^{3+}$ peptide VCNPDNPQECLLLEPGLNEIMANSL DYNER (+NEM), with highlighted fragment ion indicating the NEM modification on the cysteine residue 141. **c**, IB analysis of whole cell lysate (WCL) and anti-Flag immunoprecipitants derived from HEK293T cells transfected with c-terminal tagged ACE1 WT and CS mutants and lysed at the presence or absence of HAM.

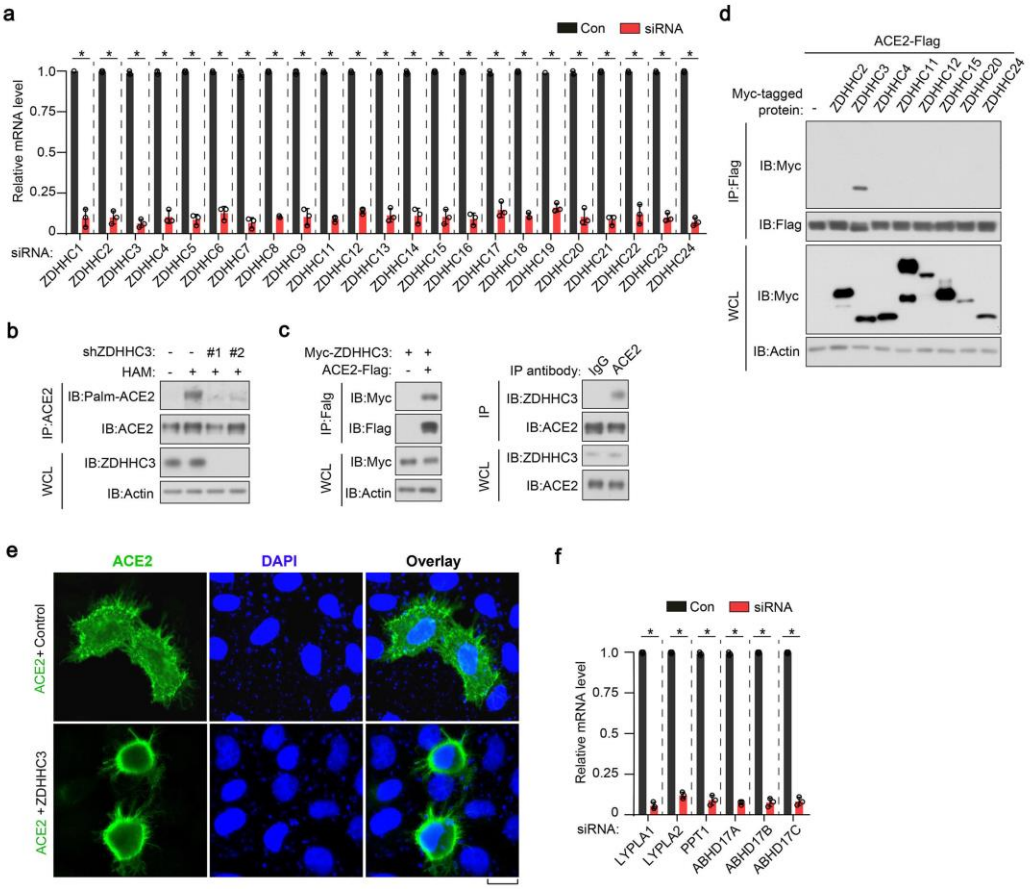

Supplementary Figure 4

Supplementary Figure 4. ACE2 interacts with ZDHHC3 palmitoyltransferase. **a**, qPCR analysis of the siRNA knockdown efficiency for ZDHHC family genes in HEK293T cells stably expressing ACE2. **b**, IB analysis of WCL and anti-ACE2 immunoprecipitants derived from HEK293T cells infected with lentivirus encoding ZDHHC3 shRNA (#1 and #2) and lysed at the presence or absence of HAM. **c**, IB analysis of WCL and immunoprecipitants from HEK293T cells transfected with expression constructs encoding ACE2-Flag and Myc-ZDHHC3 (left panel) or from non-transfected Vero-E6 cells (right panel). **d**, IB analysis of whole cell lysate (WCL) and anti-Flag immunoprecipitants from HEK293T cells transfected with ACE2-Flag and Myc-tagged ZDHHCs family proteins. **e**, Immunofluorescence and DAPI staining of HeLa cells stably expressing ZDHHC3 and transfected with ACE2. Scale bar, 20 μm. **f**, qPCR analysis of siRNA knockdown efficiency for depalmitoylase family

genes in HEK293T cells stably expressing ACE2.

*$p < 0.05$ (two-tailed Student's t test (**a**, **f**). Data are analyzed of three independent experiments and shown as mean ± SD (**a**, **f**).

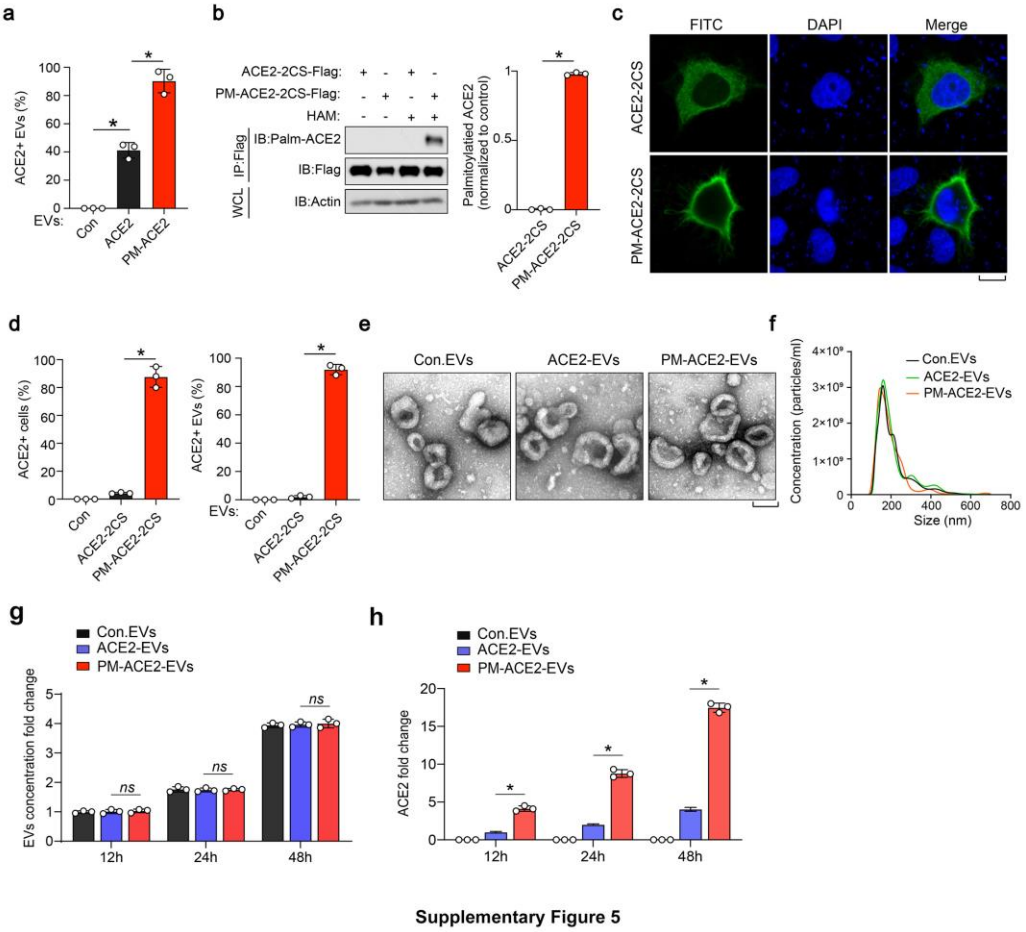

Supplementary Figure 5

Supplementary Figure 5. Analysis of purified PM-ACE2-EVs.

a, FACS analysis and quantification of purified EVs derived from HeLa cells transfected with control vector (Con.), ACE2-WT or PM-ACE2. **b**, IB analysis of whole cell lysate (WCL) and immunoprecipitants derived from HEK293T cells transfected with c-terminal Flag-tagged ACE2 2CS mutant and c-terminal Flag-tagged PM-ACE2 2CS mutant, followed by the lysis at the presence or absence of HAM (1 M). The S-palmitoylation levels of ACE2 2CS mutant and PM-ACE2 2CS mutant were quantified of three independent experiments and shown right. **c**, Immunofluorescence and DAPI staining of HeLa cells transfected with ACE2 2CS mutant or PM-ACE2 2CS mutant. Scale bar, 10 μm. **d**, FACS analysis of HEK293T

stable cells (left) and purified EVs (right) derived from HEK293T cells stably expressing control vector (Con.), normal ACE2 2CS mutant or PM-ACE2 2CS mutant. **e**-**f**, The TEM image (**e**) and nanoparticle tracking (**f**) of purified EVs derived from MSC cells stably expressing control vector (Con.), normal ACE2 or PM-ACE2. **g**-**h**, Nanoparticle tracking (**g**) and ELISA (h) analysis of purified EVs derived from MSC cells stably expressing control vector (Con.), ACE2 or PM-ACE2.

*$p < 0.05$ (two-tailed Student's t test (**a**, **b** (right), **d**, **g**, **h**)). Data are analyzed of three independent experiments and shown as mean ± SD (**a**, **b** (right), **d**, **g**, **h**)).

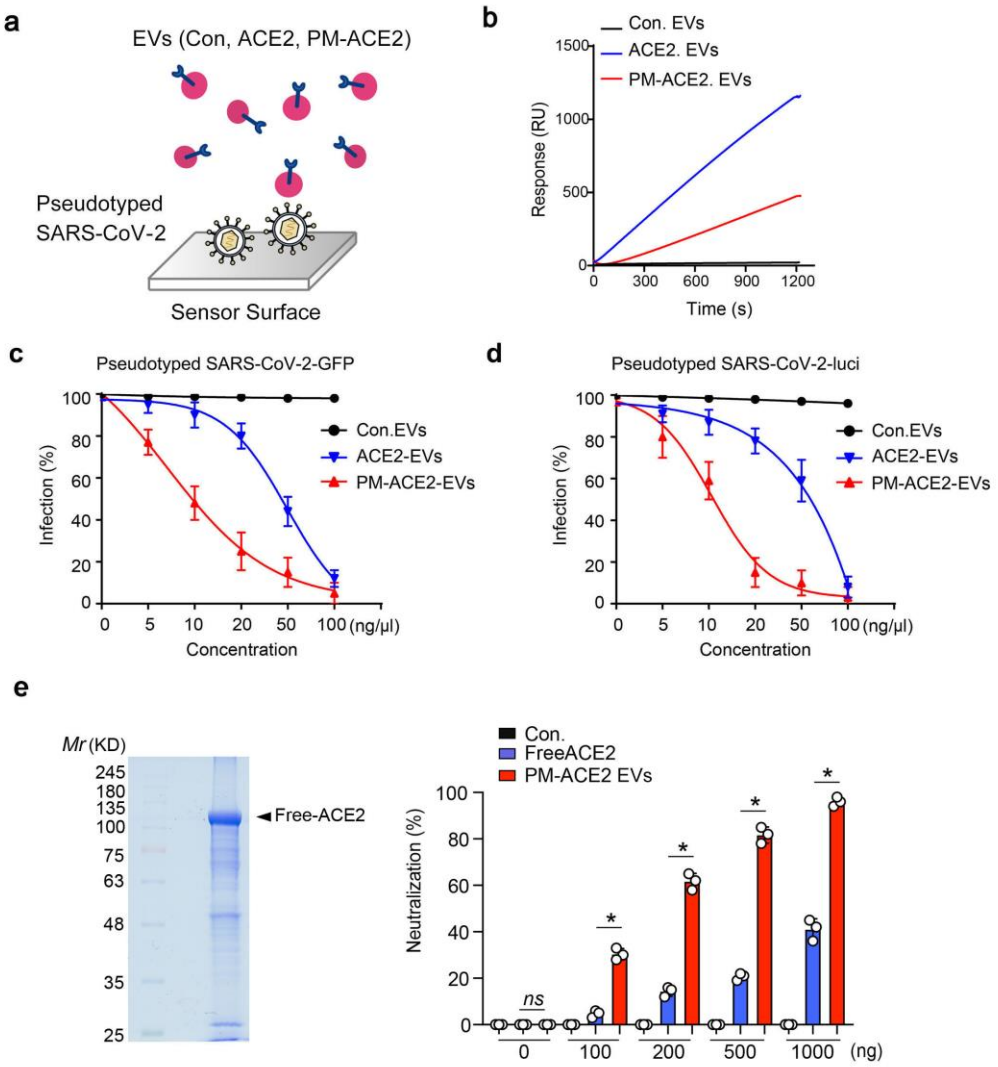

Supplementary Figure 6

Supplementary Figure 6. The neutralization potency of PM-ACE2-EVs against pseudotyped SARS-CoV-2.

a, Schematic diagram of functionalization of the surface-plasmon resonance (SPR). SARS-CoV-2 pseudovirus is immobilized on chip-gold surface at the level of 3000 RU with amine coupling standard method, and the EVs bound with SARS-CoV-2 pseudovirus will be captured. **b**, The binding affinities of ACE2-EVs and PM-ACE2-EVs with SARS-CoV-2 pseudovirus were evaluated using SPR technique. The amount of immobilized pseudovirus was approximately 3000 RU. Flow rate, 5 μL/min; EVs, 100 ng/μL. **c**-**d**, Infection curve of SARS-CoV-2-GFP pseudovirus (**c**, MOI=1) and SARS-CoV-2-luci pseudovirus (**d**, MOI=1) in Vero-E6 cells treated with

Con.EVs, ACE2-EVs or PM-ACE2-EVs at the concentration of 0, 5, 10, 20, 50, 100 ng/μl. **e**, SARS-CoV-2-luci pseudovirus neutralization assay of free ACE2 and PM-ACE2-EVs. Bacterially purified ACE2-GFP proteins were analyzed by SDS-PAGE and detected by Coomassie blue staining (left). Vero-E6 cells treated with control PBS, free ACE2 or PM-ACE2-EVs at the same amount of ACE2 (0, 100, 200, 500, 1000 ng) were infected with SARS-CoV-2-lcui pseudovirus (MOI, 1) for 24 h, and the luciferase activity was determined at 48 h post infection. The neutralization potency of control, free ACE2 and PM-ACE2-EVs was calculated based on the SARS-CoV-2-luci pseudovirus neutralization assay (right).

*$p < 0.05$ (two-way ANOVA (**c**, **d**) and two-tailed Student's t test (**e** (right))). Data are analyzed of three independent experiments and shown as mean ± SD (**c**, **d**, **e** (right)).

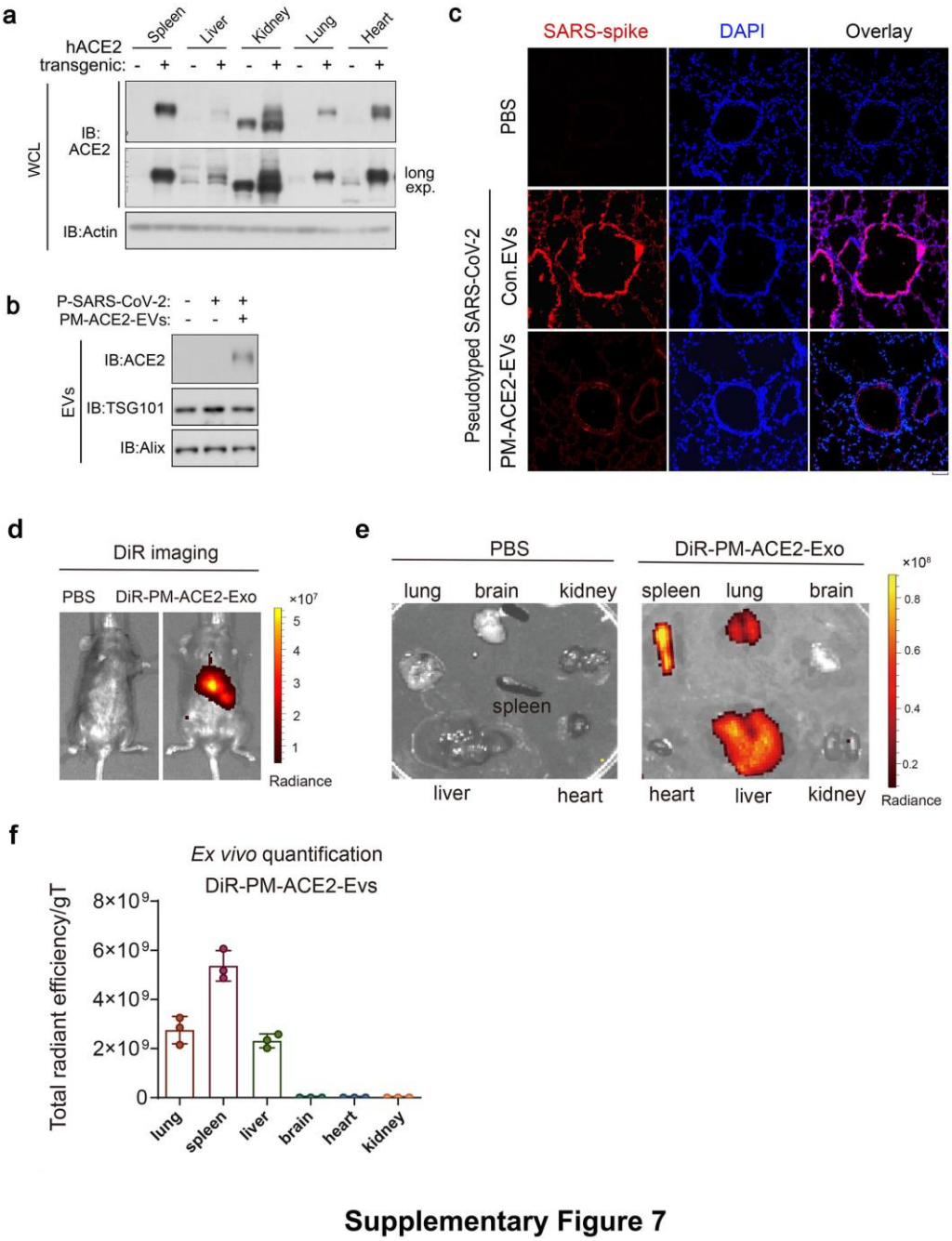

Supplementary Figure 7

Supplementary Figure 7. PM-ACE2-EVs block the infections of SARS-CoV-2 pseudovirus in hACE2 mice *in vivo*.

a, IB analysis of ACE2 protein levels in spleen, liver, kidney, lung and heart from wild type C57BL/6 mice (-) and human ACE2 transgenic mice (+). **b**, Related to Figure 7b, representative IB analysis of PM-ACE2-Flag protein level of blood circulating EVs from each group at 2 days post infection. **c**, Related to Figure 7e,

representative immunofluorescence and DAPI staining of SARS-CoV-2 spike in bronchial epithelial cells of the lungs from each group at 2 days post infection. **d-f**, *In vivo* tracking of DiR-labeled EVs in mice. Mice were intravenously injected with DiR-labeled EVs or PBS via the tail vein. In vivo imaging analysis and tissue quantifications were performed at 24 h post administration. Representative *in vivo* images of PBS-treated or DiR-EV-treated mice (**d**). Major organs (brain, heart, lungs, liver, spleen, kidneys) were excised and imaged *ex vivo*. Representative *ex vivo* images of whole organs are shown (**e**). Semiquantitative analysis of the organ biodistribution profile from ex vivo imaging of DiR EV-treated mice (**f**). Individual ROIs were drawn for each organ to obtain their respective DiR fluorescence signals. Background signals from the PBS-treated mice were subtracted from the data. Fluorescent signal is represented as total radiant efficiency [p/s]/[μW/cm^2] per gT. Values are expressed as mean ± standard error of mean; n = 3 for all groups. *$p < 0.05$ (two-tailed Student's t test (**f**)). Data are analyzed of three independent experiments and shown as mean ± SD (**f**).

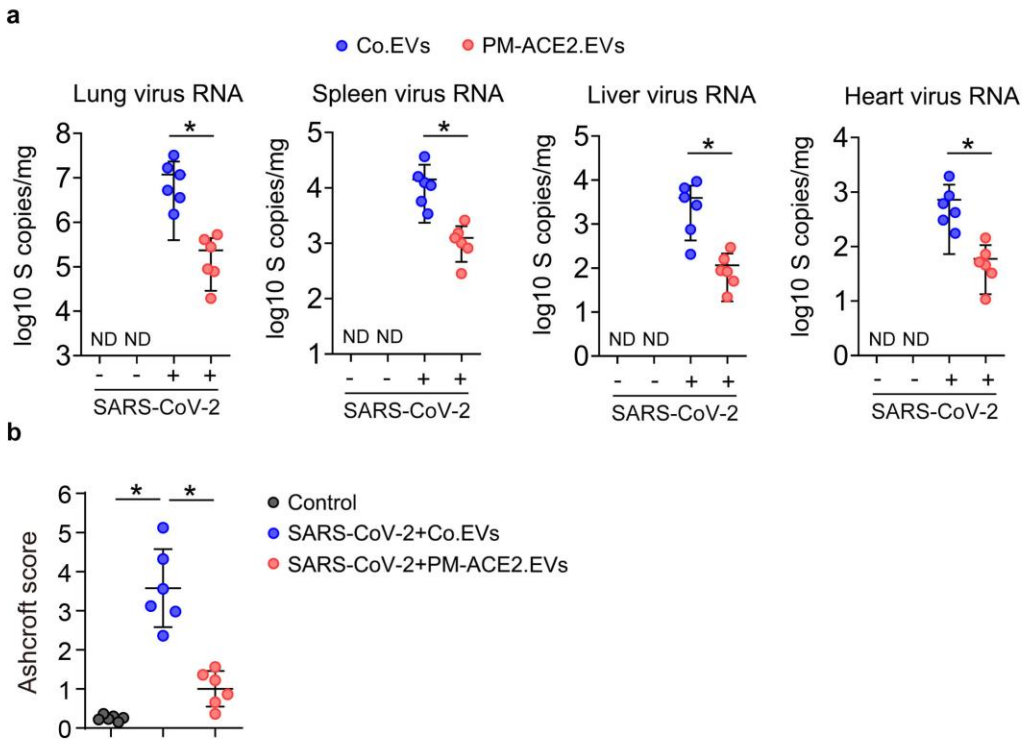

Supplementary Figure 8

Supplementary Figure 8. PM-ACE2-EVs block the infections of authentic SARS-CoV-2 in hACE2 mice.

a, qPCR analysis of authentic SARS-CoV2 S gene in the lung, spleen, liver and heart of ACE2 transgenic mice as in Fig. 8a. **b**. Fibrotic score (Ashcroft score) was obtained with a continuous numerical scale for determining the degree of fibrotic changes in the lung among different experimental groups as in Fig. 8a.

*$p < 0.05$ (two-tailed Student's t test (**a**, **b**)). Data are analyzed of three independent experiments and shown as mean ± SD (**a**, **b**).